

# A multichannel seismic study of lithospheric flexure across the Hawaiian–Emperor seamount chain

A. B. Watts\*, U. S. ten Brink\*, P. Buhl & T. M. Brocher†

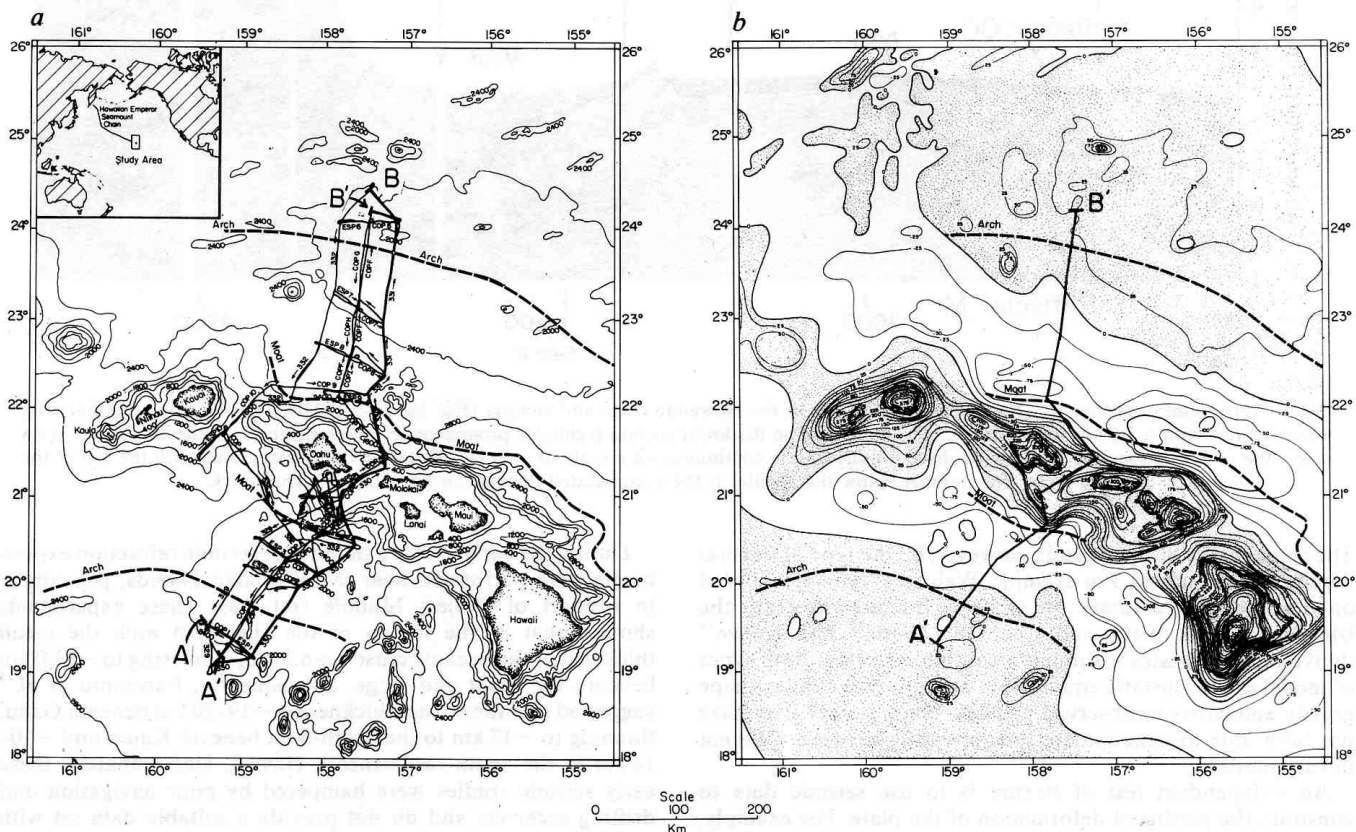
Lamont-Doherty Geological Observatory and \* Department of Geological Sciences, Columbia University, Palisades, New York 10964, USA

† Woods Hole Oceanographic Institution, Woods Hole, Massachusetts 02543, USA

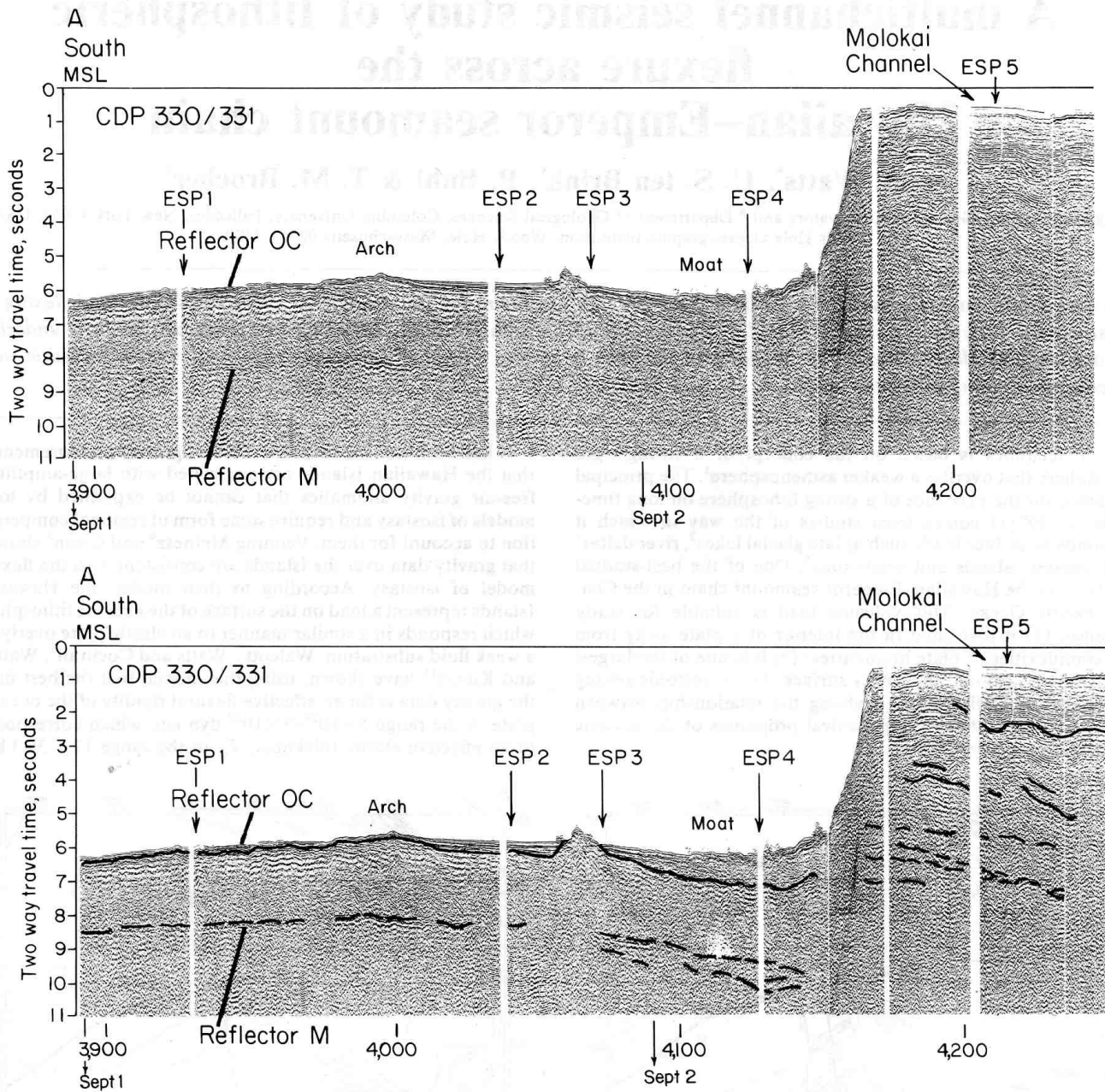
*Existing models assume that the thickened crust beneath seamounts is the result of a surface volcanic load flexing an elastic plate. New results suggest that flexed oceanic crust beneath the Hawaiian–Emperor seamount chain is underlain by a 4-km thick deep crustal body. We interpret the body as a deep crustal sill complex associated with the tholeiitic stage of volcano building along the chain.*

PLATE tectonics is based on the concept of a strong rigid lithosphere that overlies a weaker asthenosphere<sup>1</sup>. The principal evidence for the existence of a strong lithosphere on long time-scales ( $>10^6$  yr) comes from studies of the way in which it responds to surface loads such as late glacial lakes<sup>2</sup>, river deltas<sup>3</sup> and oceanic islands and seamounts<sup>4</sup>. One of the best-studied loads<sup>5–11</sup> is the Hawaiian–Emperor seamount chain in the Central Pacific Ocean. This volcanic load is suitable for study because: (1) it is located in the interior of a plate away from the complexities of plate boundaries; (2) it is one of the largest loads ( $\sim 10^{18}$  kg) on the Earth's surface; (3) its tectonic setting is reasonably well known, enabling the relationship between load age and the thermo-mechanical properties of the oceanic lithosphere to be examined.

It has been known since the earliest gravity measurements<sup>12</sup> that the Hawaiian Islands are associated with large-amplitude free-air gravity anomalies that cannot be explained by local models of isostasy and require some form of regional compensation to account for them. Venning Meinesz<sup>4</sup> and Gunn<sup>5</sup> showed that gravity data over the islands are consistent with the flexure model of isostasy. According to their model, the Hawaiian Islands represent a load on the surface of the oceanic lithosphere which responds in a similar manner to an elastic plate overlying a weak fluid substratum. Walcott<sup>7</sup>, Watts and Cochran<sup>8</sup>, Watts<sup>10</sup> and Kunze<sup>11</sup> have shown, using this model, that the best fit to the gravity data is for an effective flexural rigidity of the oceanic plate in the range  $5 \times 10^{29}$ – $5 \times 10^{30}$  dyn cm, which corresponds to an effective elastic thickness,  $T_e$ , in the range 17.8–38.3 km.



**Fig. 1** Location map of the two-ship multichannel seismic experiment, *a*, Bathymetry; *b*, free-air gravity anomaly. In *a*, the contour interval is 400 fathoms (1 fathom = 1.8288 m) and is based on Chase *et al.*<sup>34</sup>. Fine track lines, location of individual CDP, COP and ESPs; heavy line, location of ESP 1/COP 1 (Fig. 3) and CDP 330/CDP 331 (Figs 1, 2, profile AB); A'B', end points of the free-air gravity anomaly and bathymetry profile connecting ESP mid-points. In *b*, the contour interval is 25 mgal (1 mgal = 0.001 cm s<sup>-2</sup>) and is based on Watts and Talwani<sup>35</sup>. Gravity anomalies > 25 mgal are stippled. Thick dashed lines in *a* and *b* indicate the location of the Hawaiian arch and moat based on all available bathymetry profiles in the region.



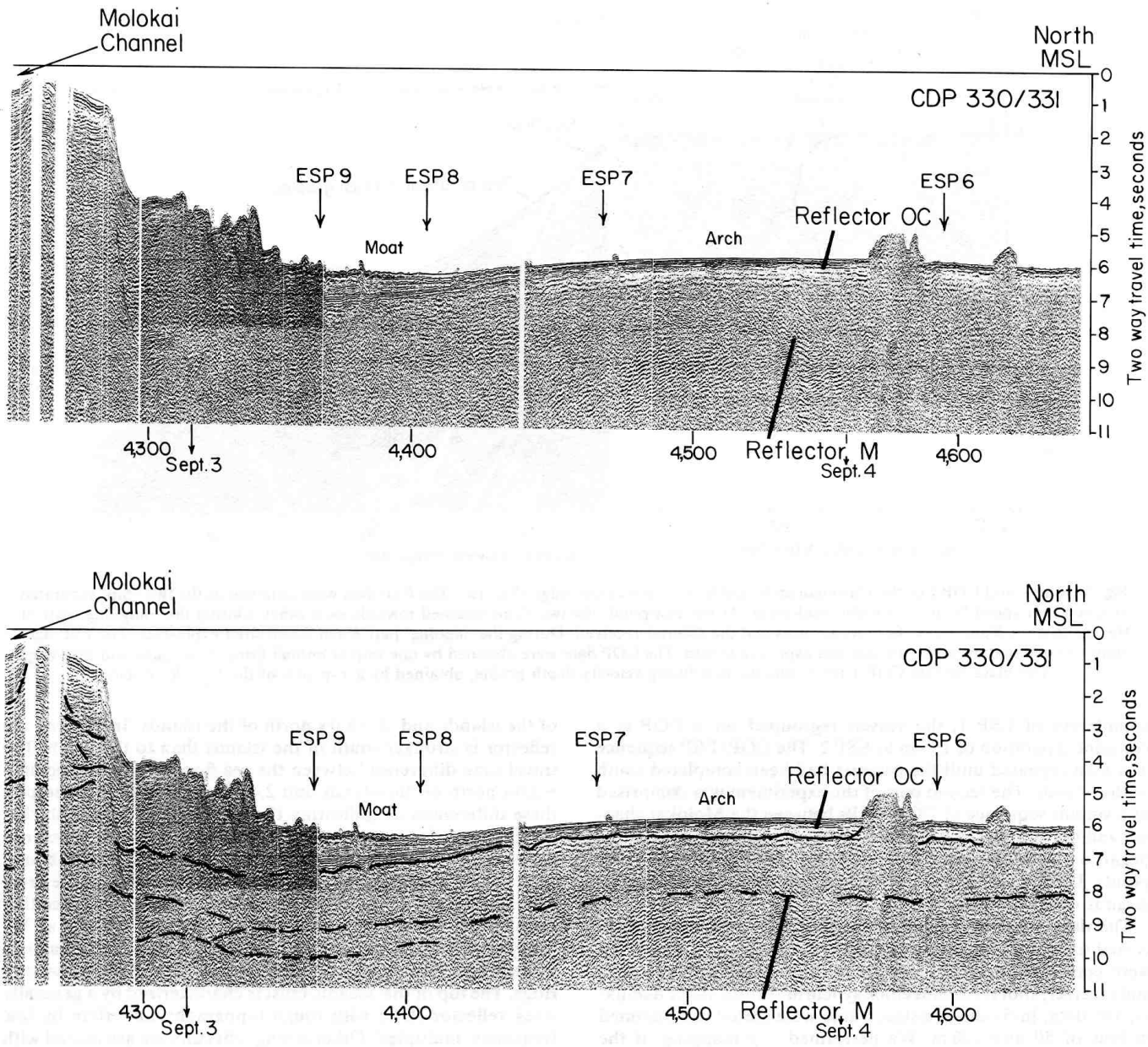
**Fig. 2** (Above and opposite) CDP profiles 330 and 331 of the Hawaiian ridge and vicinity (Fig. 1a, profile AB). The 48-fold stacked section was acquired with a 3.6-km towed array. The black line on the lower section highlights prominent seismic reflectors. Reflector M at ~8.2 s below the arch is associated with the *M*-discontinuity and is continuous on a scale of ~50 km. Reflector OC is associated with the top of the oceanic crust. The number below the profiles is the accumulated distance in km along the ship track.

The actual value of  $T_c$  depends, however, on the type of flexural model that is assumed. For example, Walcott's<sup>7</sup> estimate is based on a model that assumes the plate is fractured beneath the islands, whereas Watts and Cochran<sup>8</sup>, Watts<sup>10</sup> and Kunze<sup>11</sup> derive their estimates assuming a continuous plate. Both types of model are in isostatic equilibrium and produce similar shape gravity anomalies to observed profiles. Thus, gravity data have not been able to discriminate unequivocally between different flexure models.

An independent test of flexure is to use seismic data to constrain the predicted deformation of the plate. For example, Walcott<sup>7</sup> predicted that normal thickness oceanic crust is flexed by ~13 km beneath Oahu, whereas Watts<sup>10</sup> and Kunze<sup>11</sup> predicted only ~4 km. If the thickness of the oceanic crust in undeformed regions is 6 km, then these authors imply a depth to the *M*-discontinuity of 23.5 and 14.5 km for the fractured and continuous plate models, respectively.

During the early 1960s, a number of seismic refraction experiments were performed near the Hawaiian Islands, principally in support of Project Mohole (ref. 13). These experiments showed that in the region of the Hawaiian arch the mean thickness of the oceanic crust is ~6.3 km, increasing to ~13.0 km beneath the moat and ridge. Subsequently, Furomotu *et al.*<sup>14</sup> suggested that the crustal thickness is ~19–20 km beneath Oahu, thinning to ~17 km to the north-west beneath Kauai and ~10–14 km to the south-east beneath Hawaii. Unfortunately, these early seismic studies were hampered by poor navigation and drifting receivers and do not provide a suitable data set with which to constrain reliably the flexure model.

The purpose of this article is to summarize the results of a two-ship multichannel seismic experiment over the Hawaiian-Emperor seamount chain near the islands of Oahu and Molokai. A more detailed description of all the data obtained during the experiment will appear elsewhere (U. ten B. *et al.*, in prepar-



ation). The overall objective of the experiment was to define the detailed crustal and upper mantle velocity structure beneath a mid-plate volcanic island chain. We examine here the implications of the seismic experiment for the long-term ( $>10^6$  yr) thermo-mechanical properties of the oceanic lithosphere and petrological models for the evolution of mid-plate oceanic volcanoes.

**Seismic experiment**

During August–September 1982, the Lamont–Doherty Geological Observatory and the Hawaii Institute of Geophysics carried out a two-ship seismic experiment near Oahu and Molokai in the Hawaiian Islands (Fig. 1). The experiment involved two vessels, the *Robert D. Conrad* and *Kana Keoki*, and used the single-ship multichannel seismic reflection profiling technique<sup>15</sup> to determine the configuration of individual crustal layers and the *M*-discontinuity and the two-ship technique<sup>16</sup> to determine the detailed velocity structure of the crust and upper mantle. The *Conrad* was equipped with a 3.6-km long seismic engineering multichannel streamer with 48 active channels and a large-volume (2,500 in<sup>3</sup>) high-pressure sound source. *Kana Keoki* was equipped with a single-channel streamer, a large-volume (2,000 in<sup>3</sup>) high-pressure sound source and 210 60-pound Tovex

charges. Navigation for each ship was by satellite. During the two-ship portion of the experiment, the range between the two vessels was continuously measured by Miniranger and Raydist systems.

The seismic experiment consisted of normal incidence common depth point (CDP) data, constant offset profiles (COPs) and eleven expanding spread profiles (ESPs) obtained across a 600-km long, 100 km wide ‘transect’ of the Hawaiian ridge centred near Oahu (Fig. 1). The first part of the experiment included a continuous 250-km long COP between the Molokai channel and the Hawaiian arch south of the Hawaiian Islands (Fig. 1a). While shooting the COP, the two vessels maintained a constant distance apart of 3.6 km and *Conrad* and *Kana Keoki* alternately fired their airguns each minute. At the end of the COP, the vessels re-grouped for an ESP (Fig. 1a, ESP 1). During the ESP, the two vessels separated from each other at a speed of ~5 knots while *Kana Keoki* fired its large airguns each minute and *Conrad* received. At the end of the 65–90-km-long line, the two vessels turned and moved toward each other along the same profile. The ESP was then reshoot with the *Kana Keoki* firing Tovex charges on a 10-min schedule. During the ESP re-shoot, *Conrad* fired its airguns each minute (with each 10-min shot missing) so that a CDP profile was obtained along the ESP. On

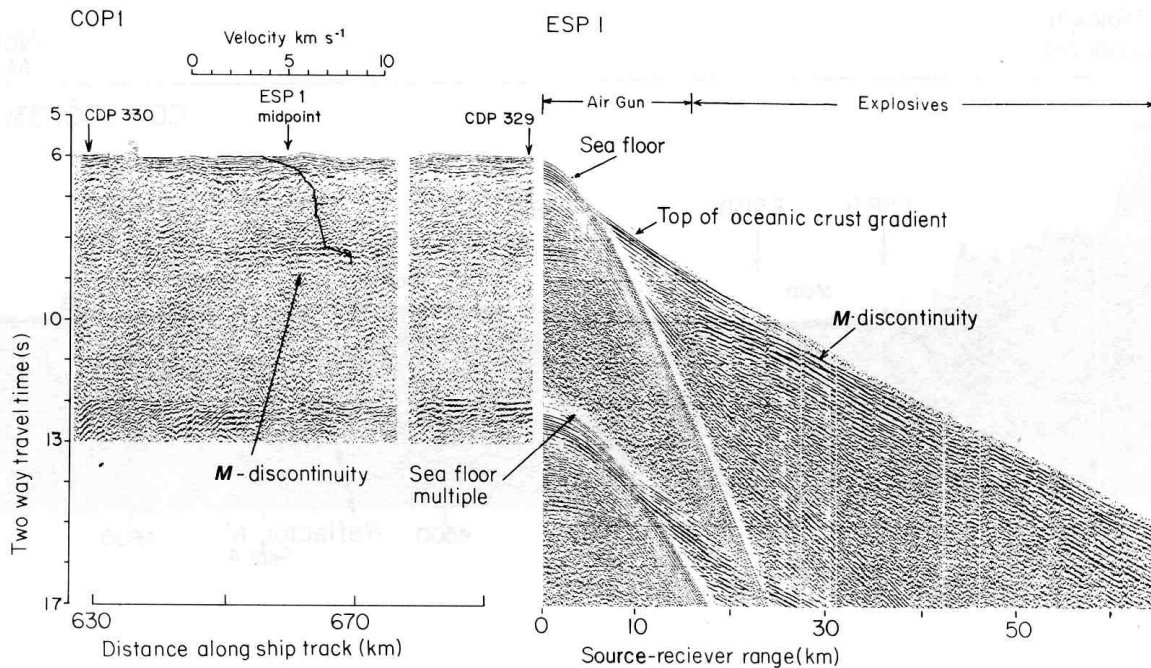


**Fig. 3** ESP 1 and COP 1 of the Hawaiian arch, south of the Hawaiian ridge (Fig. 1a). The ESP data were obtained as the two ships separated at a constant speed from a common mid-point. At the end-point, the two ships steamed towards each other. During the 'outgoing' part of the experiment *Kana Keoki* fired its air guns and the *Conrad* received. During the 'ingoing' part *Kana Keoki* fired explosives. The ESP data shows a combination of the air gun and explosive record. The COP data were obtained by one ship (*Conrad*) firing its air guns and receiving. The black line on COP 1 represents the best-fitting velocity depth profile, obtained by a  $\tau$ - $p$  sum of the ESP  $X$ - $T$  data.

completion of ESP 1, the vessels regrouped for a COP at a constant separation of 16 km to ESP 2. The COP/ESP sequence was then repeated until the transect had been completed south of the islands. The second part of the experiment was comprised of a similar sequence of COP/ESPs between the Molokai channel and the arch to the north. On completion of ESP 11, *Conrad* began a 1,200-km long CDP profile connecting the ESP end-points. During this portion of the experiment, *Conrad* fired its airguns on a 20-s schedule.

The data acquired during the seismic experiment were processed using techniques described by Stoffa *et al.*<sup>17</sup>. The ESPs were corrected for ship's navigation, the ranges between shot and receiver, shot times and clock synchronization. After demuxing the data, individual seismic traces were sorted and summed in bins of 50 and 100 m. We performed  $\tau$ - $p$  mapping of the stacked  $X$ - $T$  data and carried out a  $\tau$ -sum inversion (assuming horizontal homogeneous layers) on the  $\tau$ - $p$  data to yield a velocity-depth function at each ESP mid-point<sup>17</sup>. The solutions from  $\tau$ -sum inversion were verified by forward modelling of first arrivals using velocity gradients and accounting for spherical losses. Also, the velocity-depth function was compared with the results of semblance analysis of CDP data near some ESP mid-points and the two-way travel time data on the CDP profile that crossed each ESP mid-point. The CDP data were processed using routine methods with some exceptions. Before stacking, velocity filtering was performed on parts of the profiles, each CDP gather was muted and the first and last traces eliminated. This additional processing removed multiples of the sea floor and sub-bottom reflectors and reduced the scattered energy associated with irregularities in each reflector. After stacking and predictive deconvolution, time-varying band pass filtering was applied to all the CDP data.

## Results

We present here selected profiles of the ESP and CDP data gathered during the seismic experiment. Figure 2 shows CDP profiles 330 and 331 obtained by *Conrad* on a transect of the Hawaiian ridge between Oahu and Molokai (Fig. 1a). The figure shows a strong reflection (reflector M) from the  $M$ -discontinuity at  $\sim 8.2$  s two-way travel time beneath the Hawaiian arch south

of the islands and at  $\sim 8.0$  s north of the islands. In general, the reflector is stronger south of the islands than to the north. The travel time difference between the sea floor and the reflector is  $\sim 2.0$  s north of the islands and 2.4 s to the south. We interpret these differences as indicating that the oceanic crust is thicker south of the islands than to the north. The travel-time difference between the sea floor and reflector M increases from the arch to the moat indicating an increase in the thickness of the crust beneath the moat. At  $\sim 4,070$  km (Fig. 2), there is evidence that reflector M 'splits' at a two-way travel time of  $\sim 9.1$  s. We interpret this split in the  $M$ -discontinuity as the result of a deep crustal layer underlying the oceanic crust beneath the moat and ridge. The top of the oceanic crust is characterized by a generally weak reflector (OC) with rough topography underlain by low frequency 'multiples'. Other strong reflectors are associated with the poor-to-well stratified material of the moat infill.

Figure 3 shows ESP 1 (Fig. 1a) obtained by *Conrad* and *Kana Keoki* near the Hawaiian arch south of the islands. The right-hand side of the figure shows a line of refracted arrivals which are nearly tangential to the top of oceanic crust and  $M$ -discontinuity reflectors. There are departures, however, from straight refraction lines. For example, at ranges of 5–25 km there is a convex downward curvature of the primary refracted arrivals, suggesting a continuous increase in velocity with depth, while at  $\sim 27.5$  km there is a gap in primary arrivals, suggesting an abrupt decrease in the velocity gradient with depth. The CDP profile (Fig. 3) shows a strong reflector associated with the  $M$ -discontinuity between 8.15 and 8.45 s. The solid line at the ESP 1 mid-point on the CDP is the velocity-depth function obtained by  $\tau$ - $p$  mapping of the  $X$ - $T$  data and  $\tau$ -sum inversion. The velocity-depth function shows a progressive increase from 2.5 to 8.1 km s<sup>-1</sup>. Abrupt changes in the velocity gradient are associated with the top of the oceanic crust and the  $M$ -discontinuity.

The principal results of the CDP data and ESPs 1–9 are summarized in Fig. 4. The velocity-depth data at each ESP mid-point and the depth to prominent reflectors on CDP 330/331 have been projected onto bathymetry profile A'B' (Fig. 1a). Figure 4 shows that the total crustal thickness increases from  $\sim 6.5$  to 6.8 km beneath the Hawaiian arch to  $\sim 10.5$ –12.0 km

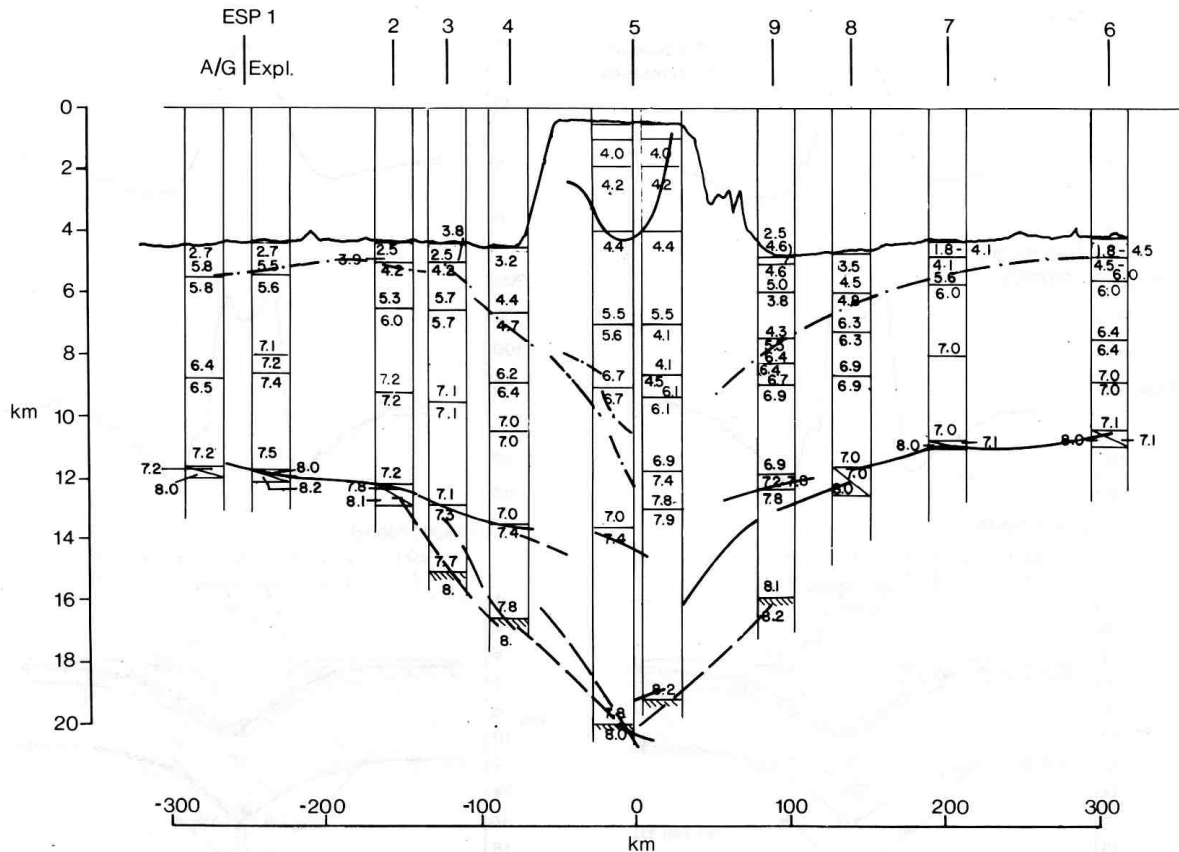


**Fig. 4** Summary of the velocity and crustal structure obtained on ESPs 1-9. Horizontal lines in each column represents the depth to a prominent change in velocity with depth. The numbers refer to the velocity ( $\text{km s}^{-1}$ ) immediately above and below the velocity change. The dashed-dot, continuous, and dashed lines represent prominent reflectors in Fig. 2 which have been converted to depth using the ESP velocity data results. These three reflectors are interpreted as corresponding to the top of the oceanic crust, the base of the pre-flexed oceanic crust and the *M*-discontinuity respectively. The ESP data have been plotted at the intersection of each ESP with profile A'B'. Note that two possible solutions are shown for ESP1 and ESP5.

beneath the moat, and 18.0-19.0 km beneath the ridge. In the region of the arch, the crustal layer below reflector OC has a velocity which grades from 4.2 to 5.6  $\text{km s}^{-1}$  (ESP 1, 2, 6, 7) to ~8.0-8.2  $\text{km s}^{-1}$ . Below reflector OC in the moat there is a sudden increase in velocity from 7.0 to 7.4  $\text{km s}^{-1}$  at depths of 6.5 km below the sea floor (ESP 4) and from 6.9 to 7.2  $\text{km s}^{-1}$  at 7.0 km to the north (ESP 9). At ESP 5 on the ridge, reflector OC cannot be as easily identified. Furthermore, the *X-T* data cannot be interpreted in terms of a single velocity-depth profile. Figure 4 shows two possible solutions for ESP 5, both showing a similar upper crustal structure with velocities increasing from 4.0 to 5.5  $\text{km s}^{-1}$ . At greater depths, however, the two solutions differ. The solution, which does not include a low-velocity zone (LVZ) in the upper crust, is characterized by a sudden increase in velocity from 7.0 to 7.4  $\text{km s}^{-1}$  at depths of ~13.0 km below the sea floor, whereas the model with a LVZ shows a sudden increase from 6.9 to 7.4  $\text{km s}^{-1}$  at depths of ~11.3 km. Above reflector OC, velocities are generally in the range 2.3-4.0  $\text{s}^{-1}$ . At ESP 9 in the moat region, there is evidence from arrivals on *X-T*,  $\tau$ -*p* and from amplitude data for a LVZ above reflector OC. We interpret this LVZ as the result of a high-velocity lava flow capping low-velocity material of the moat infill.

To constrain better the crustal model, we computed the gravity and geoid effect of the seismic structure and compared it with the observed free-air gravity anomaly profile obtained on *Conrad* and *Kana Keoki* and the geoid anomaly derived from SEASAT radar altimeter data. Because of uncertainties in the seismic interpretation at ESP 5 (Fig. 4), two models for the deep crustal structure of the ridge were considered: one in which the oceanic crust is thinned beneath the ridge (Fig. 5, model A) and one in which the crust is of normal thickness (Fig. 5, model B). Model A is consistent with the solution without a LVZ in the upper crust, whereas model B agrees better with the solution with a LVZ. For the purposes of the gravity and geoid calculation, the

velocity-depth data near the arch and moat were generalized to an upper 4.2-6.0- $\text{km s}^{-1}$  layer, a middle 6.0-7.1- $\text{km s}^{-1}$  layer and a lower 7.4-7.8- $\text{km s}^{-1}$  layer. Densities of 2.6, 3.0 and 3.15  $\text{g cm}^{-3}$ , respectively, were assigned to these layers using the velocity-density relationships of Christensen and Salisbury<sup>18</sup>. We assigned a density of 2.3  $\text{g cm}^{-3}$  for the material filling the moat, a density similar to the average density of vesicular Hawaiian flows<sup>19</sup> and in the range of values normally chosen for sediments. At ESP 5, the volcanic 'core' of the ridge is associated with velocities of 4.0-6.7  $\text{km s}^{-1}$ . A density of 2.5-2.7  $\text{g cm}^{-3}$  was assigned for the core of the ridge, similar to values normally considered for volcanic flows<sup>19</sup>.

Figure 5 shows that there is a good overall agreement between the observed and the calculated gravity and geoid anomalies based on the seismic structure. Gravity and geoid data agree with the suggested thickening of the crust from ~6.5 km beneath the arch to 12.0 km beneath the moat and 18.0-19.0 km beneath the ridge. Furthermore, the data are consistent with the existence of a deep crustal layer underlying oceanic crust beneath the ridge and a portion of the flanking moat. The data cannot, however, distinguish whether the oceanic crust is thinned beneath the ridge or whether it has a similar thickness as beneath the moat and arch. Figure 5 shows that if oceanic crust is normal thickness beneath the ridge a high density body is required beneath it to compensate for the additional low density associated with the increase in thickness of the oceanic crust. The origin of the body is not clear, but gravity modelling suggests that it represents a deep seated extension of the dense volcanic pipe associated with the Koolau caldera on Oahu<sup>20</sup>.

## Implications

The seismically determined crustal structure of the Hawaiian ridge has implications for both the thermo-mechanical

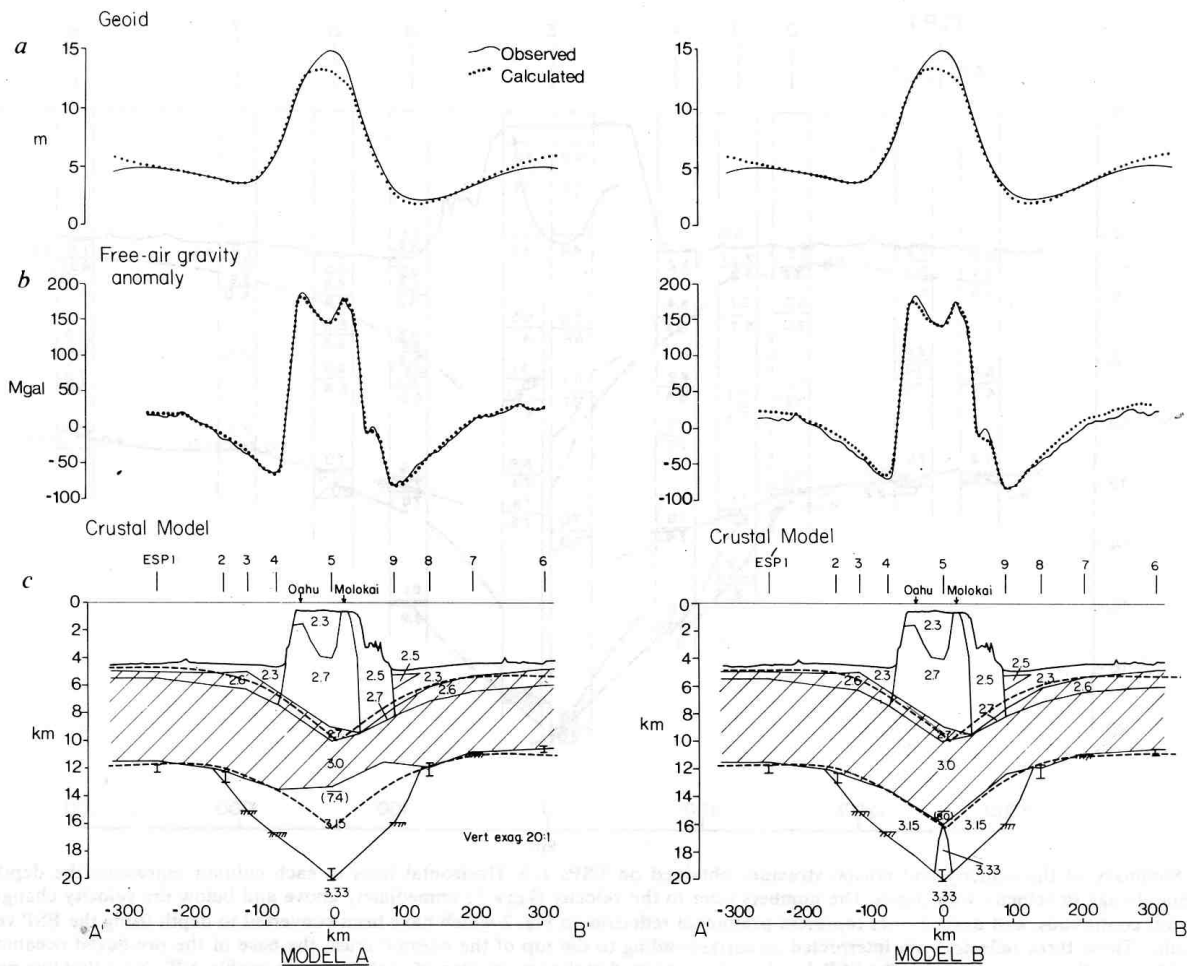


**Fig. 5** Comparison of calculated geoid and gravity anomaly based on a density model constrained by seismic data to observed satellite derived geoid and surface-ship free-air gravity anomaly data. *a*, Geoid anomaly obtained by subtracting the geoid derived from a descending track of SEASAT from the GEM 10 Earth model complete to degree and order 12. *b*, Free-air gravity anomaly profile derived from data obtained by *Conrad and Kana Keoki* during COP A/COP B and COP E/COP F. *c*, Density model based on velocity-depth data in ESPs 1-9 and the velocity-density relationships of *Christensen and Salisbury*<sup>19</sup>. The configuration of the models (see text) have been adjusted so as to best-fit the gravity and geoid data and still explain the seismic data. Model A, thinned oceanic crust; model B, normal thickness oceanic crust. Heavy dashed lines are calculated curves based on a flexure model of isostasy with  $T_e = 25$  km.

properties of oceanic lithosphere and petrological models for the evolution of mid-plate seamount chains.

The configuration of the oceanic crust near Oahu and Molokai is compared with predictions based on a flexure model of isostasy described in Fig. 5. In the model, it is assumed that the Hawaiian ridge and its associated infill material represent a two-dimensional load on the surface of an elastic plate overlying a weak fluid substratum. Thus, we assume that the only loads that act on the plate are surface loads and that buried loads<sup>21</sup> do not contribute to the flexure. Figure 5 shows that there is a reasonable agreement between the configuration of the upper surface of the oceanic crust and the calculated flexure profile for  $T_e = 25$  km. There is also good agreement between the calculated profile and the configuration of the base of the oceanic crust for the model in which the oceanic crust is uniform in thickness beneath the ridge. Figure 5 shows, however, that the agreement is poor for the model in which the oceanic crust thins beneath the ridge. These results, therefore, suggest that beneath the ridge, flexed normal thickness oceanic crust is either underlain by a high density body (model B) or has been altered by densification in its lowest part (model A).

The flexure profile in Fig. 5 is based on a single value of  $T_e$  and a fractured plate model. Other values of  $T_e$  would be required if different types of flexure model are used. For example, if a continuous rather than a fractured plate had been used, then a lower value of  $T_e$  (~20 km) would be required. We prefer the fractured plate model (and hence the higher  $T_e$  value) because it best explains the shape of the top of the oceanic

crust below the moat and the edge of the load. We caution against a too literal interpretation of the  $T_e$  value in Fig. 5, however, because it may be possible to construct other models (for example, a model in which  $T_e$  decreases gradually from beneath the arch to the ridge) that could explain the seismic, gravity and geoid data (Fig. 5) equally well. A value of  $T_e = 25$  km can, therefore, be regarded as a 'best fit' to the regional crustal structure of the ridge and hence, a measure of the average response of oceanic lithosphere to volcanic island loading along the Hawaiian-Emperor seamount chain.

Oceanic flexure studies<sup>10</sup> have shown that  $T_e$  is a strong function of the age of the lithosphere at the time of loading. Thus, volcanic loads formed on young lithosphere are associated with small values of  $T_e$ , whereas loads formed on old lithosphere are associated with large values. There is a good agreement between  $T_e$  and the depth to the 450 °C oceanic isotherm based on the cooling plate model. *Bodine et al.*<sup>22</sup> have considered these results in terms of the rheology of oceanic lithosphere based on data from experimental rock mechanics and shown that

$$T_e \approx 4.3t^{1/2}, \text{ 'dry' olivine rheology} \quad (1)$$

$$T_e \approx 3.3t^{1/2}, \text{ 'wet' olivine rheology} \quad (2)$$

where  $t$  is age of the oceanic lithosphere (Myr) at the time of load emplacement. Using  $t = 80$  Myr in equations (1) and (2) gives a predicted  $T_e$  of 30-40 km, which is somewhat higher than the value of  $T_e$  deduced here.

Although  $T_e$  at a volcanic load is a function for the thermal age of the underlying oceanic lithosphere<sup>10</sup>, it may not represent the actual temperature structure of the lithosphere because of perturbing effects associated with magmatic processes and/or subsequent thermal events. Crough<sup>23</sup>, for example, suggested that the Hawaiian swell is the result of thermal uplift following reheating of oceanic lithosphere by the Hawaiian hotspot. He estimated from bathymetric data that the 80 Myr lithosphere near Hawaii has been reheated to a thermal age of ~30 Myr. Substituting this value in equations (1) and (2) gives a predicted  $T_e$  of 18–23 km, which is similar to  $T_e$  estimated here. However, Sandwell<sup>24</sup> computed the response of a moving plate over heat sources with different shapes and has shown that the peak in the temperature distribution may be displaced  $\leq 20$  Myr downstream of the source. The age of the volcanic load near Oahu and Molokai is only ~2–3 Myr, so that the  $T_e$  estimated here cannot be used to constrain the reheating hypothesis. Thus, the strongest evidence for the swell remains the exponential form of its subsidence.

Although the extent of lithospheric reheating is uncertain, it is clear that a flexure model of isostasy with  $T_e = 25$  km can explain the overall configuration of the oceanic crust near Oahu and Molokai. The model cannot, however, account for the 7.4–7.8 km s<sup>-1</sup> velocity layer which seismic, gravity and geoid data suggest underlies flexed oceanic crust beneath the islands. This deep crustal layer is ~4 km thick, 200 km wide and generally symmetric below the centre of the ridge.

It is known from petrological studies that the Hawaiian volcanoes erupt lavas of different and distinct chemical compositions during their evolution. According to McDonald<sup>25</sup>, the main stage of volcano building consists of large amounts of tholeiitic lavas which erupt rapidly ( $\leq 1$  Myr; ref. 26). Following the main stage, the volcano usually erupts small amounts of alkali basalts. Finally, after a few Myr of quiescence, minor amounts of nephelinitic lavas may erupt from satellite vents. The exact nature of the source region of the tholeiites and alkali basalts is not known<sup>27,28</sup> but seismicity studies near Hawaii<sup>29</sup> suggest that magma transfer associated with the tholeiitic stage of volcanism extends to depths of at least 50–60 km. The nephelinitic lavas are considered to be more primitive and to have originated from an even deeper source.

Seismic studies provide constraints on the velocity and density structure of the crust and upper mantle beneath a volcano and hence are of importance in developing petrological models. For example, seismic data<sup>30</sup> suggest that Mount Etna is underlain by a deep seated magma chamber.

From a consideration of all the seismic data obtained during the experiment, we believe that the most probable interpretation of the deep crustal body underlying flexed oceanic crust beneath Oahu and Molokai is that it represents a deep crustal sill complex. In particular, the body represents 'frozen' intrusions of tholeiitic composition into upper mantle rocks that were trapped in their ascent from a deeper source during the late phase of

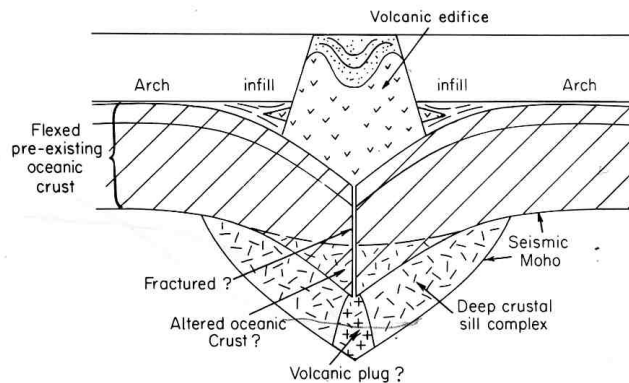


Fig. 6 Schematic model of the crustal structure of the Hawaiian ridge and vicinity based on the seismic, gravity and geoid data discussed here. The model has been generalized from models A and B in Fig. 5.

the tholeiitic stage or during the following period of quiescence. Such a model of a crust–mantle 'mix' agrees with seismic data showing that the deep crustal layer is intermediate in velocity between that of lower crust (gabbro) and upper mantle (peridotite) rocks. It is also in agreement with evidence<sup>31,32</sup> which shows an absence of a deep crustal body below Kilauea and Mauna Loa on Hawaii. These volcanoes seem to be in the early phase of the tholeiitic stage and, therefore, would not be expected to be underlain by such a sill complex.

Figure 6 shows a schematic model for the deep crustal layer beneath Oahu and Molokai that explains the geophysical data and is consistent with current petrological knowledge. In proposing this model, we have eliminated (on density arguments) the possibilities that the deep layer represents either a magma chamber of basic picritic magmas which become ponded at or near the crust/mantle following their ascent through the mantle<sup>33</sup>, or dunites and plagioclase-bearing pyroxenites that formed as early cumulates in a fractionating tholeiitic magma chamber<sup>28</sup>.

The deep structure of oceanic islands and seamounts, however, is still too poorly known and other explanations may be proposed as more data become available. The seismic experiment described here was the first of its kind to be carried out over a mid-plate seamount chain. We believe that multichannel seismic studies of other seamounts offer particular promise of better understanding the origin of mid-plate volcanism in the future.

We thank J. Mutter, J. Glasser, C. Mountain, E. Vera, D. Lindwall, C. Zehnder and the officers and crew of RVs *Conrad* and *Kana Keoki* for their help at sea and J. Mutter and J. Weissel for critical reviews. This work has been supported by NSF grants OCE 81-11704 (L-DGO) and OCE 81-17210 (WHOI). Lamont-Doherty contribution 3797.

Received 7 December 1984; accepted 21 February 1985.

- Barrell, J. J. *Geol.* **22**, 655–683 (1914).
- Walcott, R. I. *Can. J. Earth Sci.* **7**, 716–727 (1970).
- Cochran, J. R. *Bull. geol. Soc. Am.* **84**, 3249 (1973).
- Vening Meinesz, F. A. *Gravity Expeditions at Sea 1923–1938*, Vol. 4 (Netherlands Geod. Comm. Delftsche Uitgevers Maatschappij, Delft, 1948).
- Gunn, R. J. *Franklin Inst.* **236**, 373–396 (1943).
- Hamilton, E. L. *Bull. geol. Soc. Am.* **68**, 1011–1026 (1957).
- Walcott, R. *Tectonophysics* **9**, 435–446 (1970).
- Watts, A. B. & Cochran, J. R. *Geophys. J. R. astr. Soc.* **38**, 119–141 (1974).
- Walcott, R. I. in *Geophysics of the Pacific Ocean Basin* AGU Monogr. **19**, 431–438 (1976).
- Watts, A. B. *J. geophys. Res.* **83**, 5989–6004 (1978).
- Kunze, A. W. G. *Tectonophysics* **69**, T1–T8 (1980).
- Hayford, J. F. S. & Bowie, W. *Dept Commerce and Labor Spec. Publ.* **10** (Coast and Geodetic Service, Washington, D.C., 1912).
- Shor, G. G. & Pollard, D. D. *J. geophys. Res.* **69**, 1627–1638 (1964).
- Furumoto, A. S., Woollard, G. P., Campbell, J. F. & Hussong, D. M. in *The Crust and Upper Mantle in the Pacific Area* AGU Monogr. **12**, 94–111 (1968).
- Mayne, W. H. *Geophysics* **27**, 927–938 (1962).
- Stoffa, P. L. & Buhl, P. *J. geophys. Res.* **84**, 7645–7663 (1979).

- Stoffa, P. L., Diebold, J. B. & Buhl, P. *Geophys. Prospect.* **30**, 25–57 (1982).
- Christensen, N. I. & Salisbury, M. H. *Rev. Geophys. Space Phys.* **13**, 57–86 (1975).
- Manghni, M. H. & Woollard, G. P. in *The Crust and Upper Mantle in the Pacific Area*, 401–516 (American Geophysical Union, Washington, 1970).
- Strange, W. E., Woollard, G. P. & Rose, J. C. *Pacif. Sci.* **19**, 381–389 (1965).
- Karner, G. D. & Watts, A. B. *J. geophys. Res.* **88**, 10,449–10,477 (1983).
- Bodine, J. H., Steckler, M. S. & Watts, A. B. *J. geophys. Res.* **86**, 3695–3707 (1981).
- Crough, S. T. *Geophys. J. R. astr. Soc.* **55**, 451–469 (1978).
- Sandwell, D. T. thesis, Univ. Calif. Los Angeles (1981).
- MacDonald, G. A. *Mem. geol. Soc. Am.* **116**, 477–522 (1978).
- Jackson, E. D., Silver, E. A., & Dalrymple, G. B. *Bull. geol. Soc. Am.* **83**, 601–617 (1972).
- Chen, C. Y. & Frey, F. A. *Nature* **302**, 785–789 (1983).
- Sen, G. *Earth planet. Sci. Lett.* **62**, 215–228 (1983).
- Estill, R. E. thesis, Univ. Hawaii (1979).
- Sharp, A. D. L., Davis, P. M. & Gray, F. *Nature* **287**, 587–591 (1980).
- Zucca, J. J., Hill, D. P. & Kovach, R. L., *Bull. seism. Soc. Am.* **72**, 1535–1550 (1982).
- Ellsworth, W. L. & Koyanagi, R. Y. *J. geophys. Res.* **82**, 5379–5394 (1977).
- Sparks, R. S. J., Meyer, P. & Sigurdsson, H. *Earth planet. Sci. Lett.* **46**, 419–430 (1980).
- Chase, T. E., Menard, M. W. & Mammertick, J. *Bathymetry N. Pac. Charts* **7**, 8 (Scripps' Institute of Oceanography, San Diego, 1970).
- Watts, A. B. & Talwani, M. *Geol. Soc. Am. Spec. Map Ser.* MC-9 (1975).